Progress in Physics of Applied Materials 2 (2022) 93–102

Semnan University

Progress in Physics of Applied Materials

journal homepage: https://ppam.semnan.ac.ir/

Effect of Cation and anion migration toward contacts on Perovskite solar cell performance

Mehran Minbashi, Elnaz Yazdani*,

Department of Physics. Tarbiat Modares University. Tehran. Iran

ARTICLE INFO

Article history:
Received: 17 November 2022
Revised: 3 December 2022
Accepted: 17 December 2022

Keywords:
Hysteresis
ion migration
ionic flux
contact corrosion

ABSTRACT

Despite the rapid and promising progress on the perovskite solar cell efficiency of around 25.7 % in the last few years, the ion migration as an intrinsic instability has limited the practical application of these solar cells. In this work, we have modified the common drift-diffusion equations to model the experimental current-voltage (J-V) hysteresis in Perovskite solar cells. In our model, both anions and cations have been considered. Inverted hysteresis behavior in J-V characteristics and contact corrosion in perovskite solar cells have yet to be explained clearly. To address this issue, we modified ionic-electronic transport equations by adding ionic flux equations to let ions move from the perovskite layer toward contacts. Our results show a strong inverted hysteresis because of the high flux rate of anions and cations to ETL and HTL and, consequently, toward contacts. Although the ionic flux may cause the instability of the perovskite solar cells, the efficiency is increased for the cases where anions and cations flux to HTL and ETL toward contacts. In all ionic flux models, open circuit voltages (V_{oc}) are increased due to ionic accumulation at interfaces, the built-higher gradient of electric potentials at interfaces, and the modified Fermi level (modified work function-aging process).

1. Introduction

Perovskite semiconductors have received great attention due to their low cost and easy fabrication at low temperatures, which make them applicable in solar cells [1,2], LEDs [3], and other optoelectronic devices [4]. The major attention is on the application of these materials as solar cell absorbers. The rapid rise in power conversion efficiency (PCE) from 3.8% [5] to 25.7% [6] made them an important type of solar cells. However, hysteresis phenomena in current density- voltage (J-V) [7] and short-term stability [7] are the main challenges for the commercialization of these materials as long-term stable solar cell devices. Several several reasons are suggested for hysteresis behavior of Perovskite solar cells, (i) unbalanced charge extraction/ transport related to electron and hole transport materials (ETMs and HTMs), (ii) charge carriers trapping/detrapping; (iii) the ferroelectric effect; and (iv) [1] ion migration. It can be understood from studies that perovskite might not have ferroelectricity property [2,3]. The response time is about micro and milliseconds for charge carriers trapping/detrapping, which does not contribute to the time scale of hysteresis in J-V measurements [3,4]. Also, dissociation of perovskite to ions for example $MAPbI_3$ dissociation into methylamine ion (MA^+) and iodide (I^-), causes to ionic migration. Ion migration is the most important mechanism for occurring hysteresis and stability issues [8]. Recent studies have modified the Drift-Diffusion model (DDM) to investigate the ion migration effect on solar cell parameters. Almora et al. used ionic dipolar distribution to model the ion migration process, and they showed that the combination of the ionic dipolar with pre-bias shows how ions motion can alter charge accumulation and recombination [9]. Singh et al. obtained significant hysteresis in J-V by considering cation-mediated recombination in DDM [10]. Nemnes et al. showed the normal (NH) and inverted hysteresis (IH) by the dependence of J-V characterization on the pre-polling in their study [11]. Minbashi and Yazdani [12] studied the ionic migration and investigated the effect of scan rates, perovskite mobility, and pre-bias and also considered the ionic flux at interfaces of the PSK/HTL and PSK/ETL layer. Although, they explained inverted hysteresis; but they did

* Corresponding author.
E-mail address: elnaz.yazdani@modares.ac.ir

DOI: 10.22075/ppam.2022.29018.1042

not consider the ionic flux from perovskite towards other layers [12]. There are a few studies about inverted hysteresis and contact corrosion [13,14]. In those works, the origin and the physics of the experimentally obtained inverted hysteresis have not been explained in detail. They have tried to explain the root of the inverted hysteresis by measuring protocol parameters such as pre-polling bias, high voltage pre-biasing, negative pre-biasing, and other measurement circumstances. Moreover, many reports experimentally confirmed the inverted hysteresis behavior in perovskite solar cells [11] and contact corrosion [14] without dependence on measurement.

Herein, we explain the inverted hysteresis and contact corrosion with the physics of ionic flux from the PSK layer to the ETL, and HTL layers toward contacts. We have added the rate equations for anions and cations by defining the source term at the boundary of ETL/PSK and HTL/PSK, which consider anions and cations migration to ETL and HTL sides toward contacts and vice versa. Anion flux to ETL and HTL and cation flux to ETL and HTL are considered, separately.

2. Numerical modeling

The ionic flux from the PSK layer to the transport layers toward contacts is an important problem that must solve accurately. Considering these phenomena, we define ions in PSK and let them move after the operation (applying voltage and light) and flux from PSK to ETL and HTL in the duration of time and showed the movement of ions in ETL and HTL toward both contacts. The simulations are carried out by the Finite Element Method (FEM) [15]. Eqs. (1) -(3) link the Poisson equation (Eq. (1)) with the continuity equation for electrons-holes by considering (Eqs. (2) & (3)) Shockley-Read-Hall (SRH) recombination statistics [16–23].

$$\frac{d^2}{dx^2}\Phi(x) = \frac{e}{\varepsilon_0\varepsilon_r}(p(x) - n(x) + N_D - N_A + \rho_P - \rho_n) \quad (1)$$

$$-\left(\frac{1}{q}\right)\frac{\partial J_p}{\partial x} - U_p + G = \frac{\partial p}{\partial t} \quad (2)$$

$$-\left(\frac{1}{q}\right)\frac{\partial J_n}{\partial x} - U_n + G = \frac{\partial n}{\partial t} \quad (3)$$

$$J_n = qn\mu_n\nabla E_c + qD_n\nabla n - qnD_n\nabla \ln(N_c) + qnD_{n,th}\nabla \ln(T) \quad (4)$$

$$J_p = qp\mu_p\nabla E_v - qD_p\nabla p + qpD_p\nabla \ln(N_v) - qpD_{p,th}\nabla \ln(T) \quad (5)$$

$$E_c = -(V + \chi_0), E_v = -(V + \chi_0 + E_{g,0}) \quad (6)$$

$$D_n = \mu_n K_B T g_n(n/N_c) \quad (7)$$

$$D_p = \mu_p K_B T g_p(p/N_v) \quad (8)$$

$$D_{n,th} = \mu_n K_B T/q \quad (9)$$

$$D_{p,th} = \mu_p K_B T/q \quad (10)$$

Where, Φ is the electrostatic potential, e is the electrical charge, ε_r and ε_0 are the relative and the vacuum permittivity, p and n are hole and electron concentrations, N_D, N_A, ρ_p, and ρ_n are charge impurities of the donor, acceptor, distribution of holes and electrons, respectively. J_n and J_p are the electron and hole current densities. G is the generation rate calculated by the beer-lambert law [24–26]. D_n and D_p are electron and hole diffusion coefficients. $D_{n,th}$ and $D_{p,th}$ are the electron and hole thermal diffusion coefficients, respectively. g_n and g_p are the electron and hole degeneracy functions, respectively [27]. χ_0, $E_{g,0}$, V are electron affinity, band gap, and vacuum energy level, respectively. E_c, and E_v are the conduction and valence band energy levels respectively. Here, a 1D time-dependent Drift-Diffusion (DD), thus it solves the above equations by considering the boundary conditions.

2.1. Carrier transport equations with ion migration effect

In this study, the equations for anions (a^-) and cations (c^+) are coupled with drift-diffusion equations (*i.e.*, Eqs1-3) as follows:

$$-\left(\frac{1}{q}\right)\frac{\partial J_{c^+}}{\partial x} = \frac{\partial c}{\partial t} \quad (11)$$

$$\left(\frac{1}{q}\right)\frac{\partial J_{a^+}}{\partial x} = \frac{\partial a}{\partial t} \quad (12)$$

Therefore, Poisson's equation in Eq. 1 can be rewritten as:

$$\frac{d^2}{dx^2}\Phi(x) = \frac{e}{\varepsilon_0\varepsilon_r}(p(x) - n(x) + N_D - N_A + \rho_P - \rho_n + (c^+ - a^-)) \quad (13)$$

$$J_a = q\mu_a aE + qD_a\frac{\partial a}{\partial x} \quad (14)$$

$$J_c = q\mu_c cE - qD_c\frac{\partial c}{\partial x} \quad (15)$$

The neutrality condition was considered in the entire perovskite by the following equation:

$$1/l\iint a^-(x)dx = 1/l\iint c^+(x)dx = N_i \quad (16)$$

Where l is the total thickness of perovskite and N_i is ion density.

2.2. boundary condition for Ionic transport

2.2.1. No flux of Ions into ETL and HTL

Here, we have no flow of anions and cations to ETL and HTL. This model was generally used by all theoretical researchers. The equations are as follows:

$$n.J_a = 0 \quad (17)$$

$$n.J_c = 0 \quad (18)$$

Where n is the normal vector, J_a, and J_c are anion and cation current densities, respectively. Da and Dc are anion and cation diffusion coefficients, respectively.

2.2.2. Flux of Ions into ETL and HTL (our model)

For the first time, we define the flux of anions and cations into both sides of ETL and HTL, which can describe some physical background of inverted hysteresis and contact corrosion that researchers have not been able to explore numerically. In some reports, IH has been described as a J-V characterization condition, such as negative and also high bias conditions in experiments and simulations. However, we have inverted hysteresis in other experimental conditions, such as material synthesis and device configuration, etc. [28]; it is not clear to researchers why the inverted hysteresis occurred in these conditions and has not yet been modeled theoretically. In the last section, we have shown our results considering our ion flux physics. The associated equations are as follows:

$$n.\mathrm{J}_a = q(g_a - Q_a a) \tag{19}$$

$$n.\mathrm{J}_c = q(g_c - Q_c c) \tag{20}$$

Where g_a, and g_c are the boundary fluxes of anion and cation, respectively. Q_a and Q_c are the anion and cation velocities. In the last section of this paper, we define indices ae, ah, ce, and ch, which mean anion flux to ETL, anion flux to HTL, cation flux to ETL, and cation flux to HTL, respectively. The values of g_a, and g_c are in the range of:

$$\mathrm{g_a}, \mathrm{g_c} \ll \mathrm{d_{perovskite}}.\mathrm{G_{av\_psk}} \tag{21}$$

Where $d_{perovskite}$ is the thickness of perovskite and G_{av_psk} is the average generation rate of perovskite (about 10^{22} 1/(cm^3.s)).

2.3 validation

A structure of Au/Spiro-OMeTAD/$MAPbI_3$/TiO_2/FTO (nip) [29] was used for the simulation (Fig. 1(a)). In the following, this structure was used as the reference cell for all types of perovskite compositions (our assumption), and we have considered all possible ionic migrations in our simulations. As can be seen, the simulated J-V is in good agreement with the experimental ones.

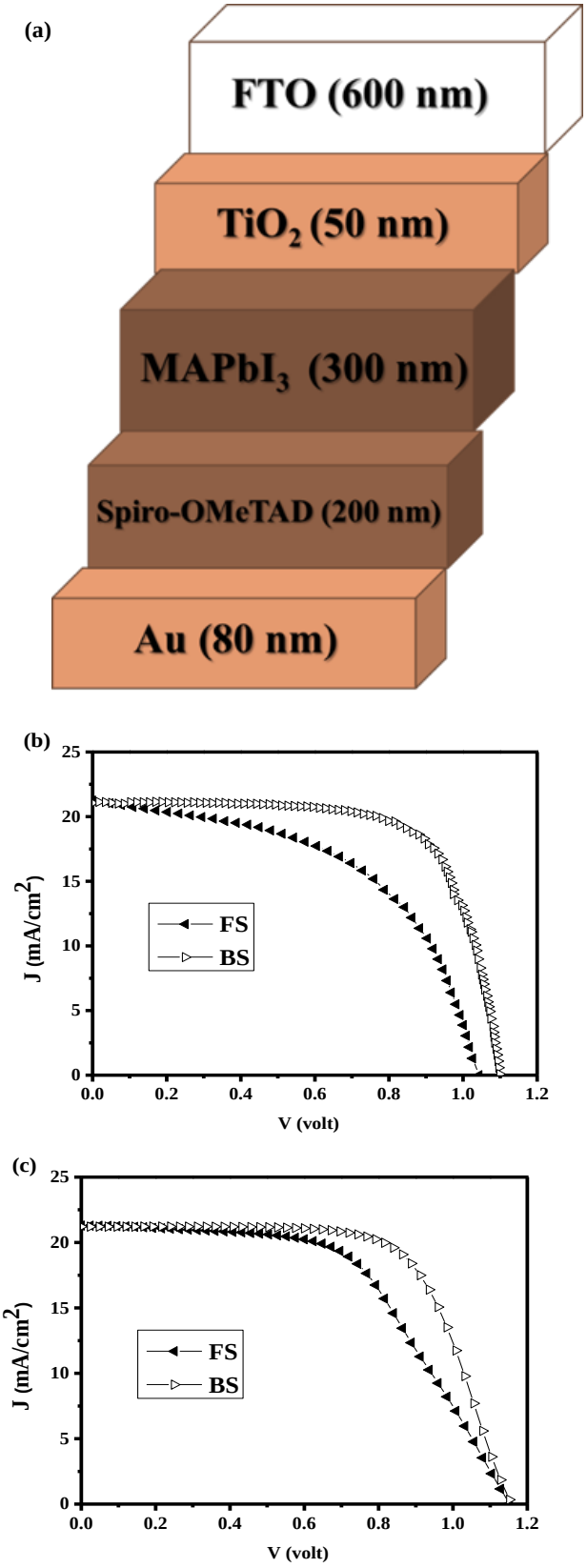

Fig. 1. (a) Schematic of perovskite solar cells used for the simulation. J–V characteristics, for (b) experimental [29], and (c) simulation. The scan rate was 100 mV/s for both cases.

The input data for the simulation of Figure 1 (c) was taken from a valid reference [12].

3. Results and discussion

Effect of dynamic ion flux on ETL and HTL

For the simulations, both contacts were considered ohmic. A schematic of anion and cation migration into the ETL and HTL sides towards the contact layers is shown in Figure 2 In this section, we investigate the effects of different ionic movements from the PSK layer toward the contacts, which still need to be simulated. In experimental work, this behavior can occur and lead to severe hysteresis, contact corrosion, and degradation of perovskite solar cells [30]. In the following section, we consider both anion and cation migration to the ETL and HTL contacts separately. At t=0 s, there are no ions on the ETL and HTL sides. The data range was chosen based on the readable change in the J-V value.

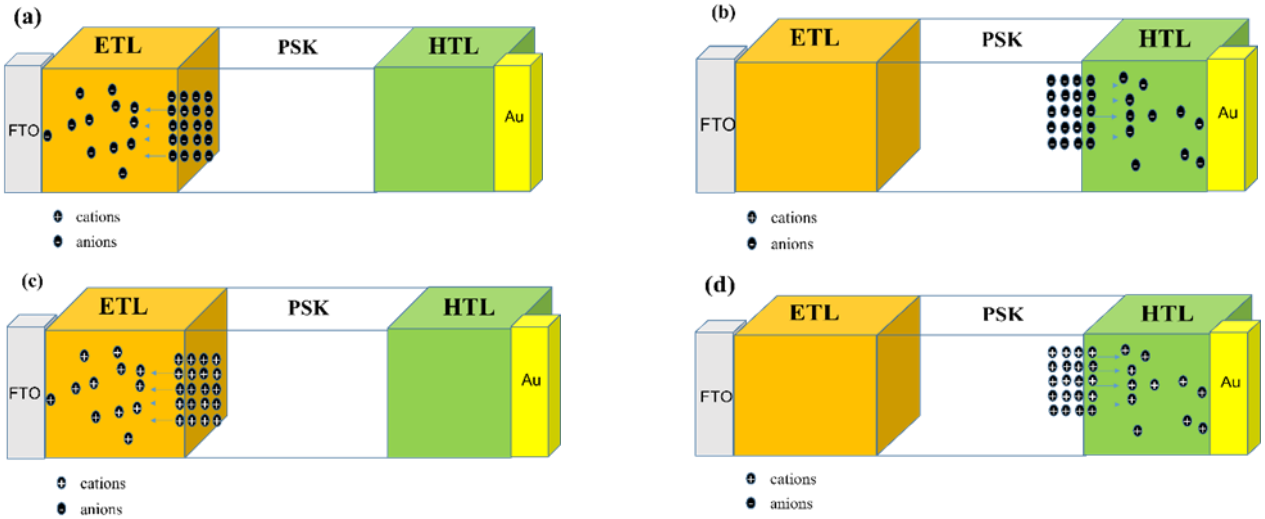

Fig.2. schematic of ionic migrations. Anions flux to (a) ETL and (b) HTL side toward contact. Cations flux to (c) ETL and (d) HTL side toward contact.

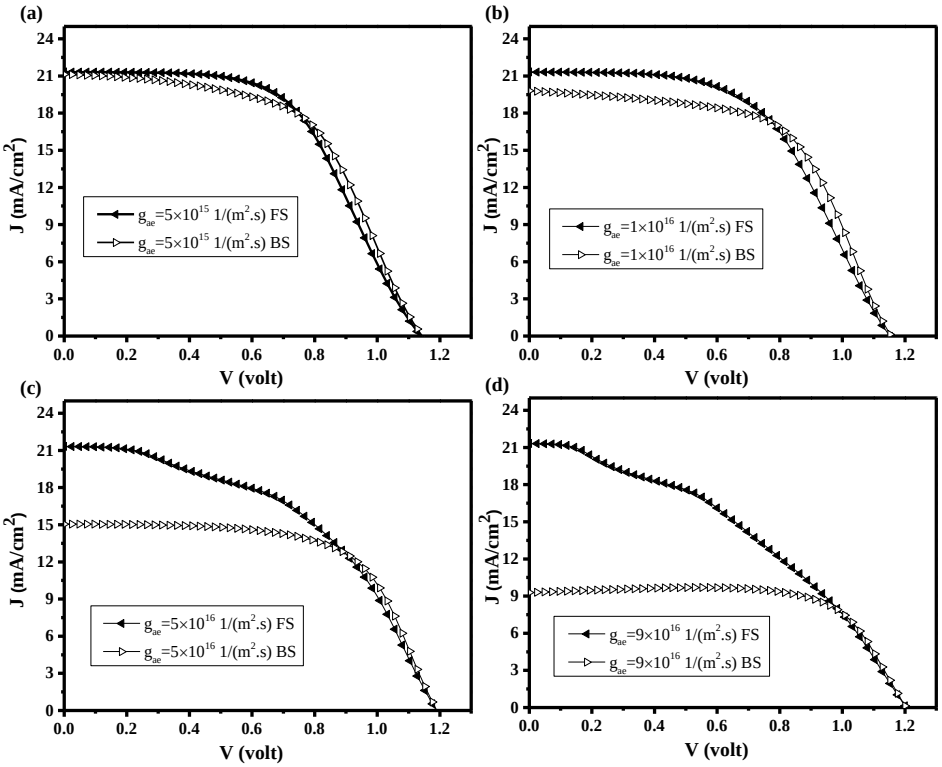

Fig. 3. Effect of different anion flux rates to ETL on J-V characteristics for (a) $g_{ae}=5\times10^{15}$ 1/ m².s, (b) $g_{ae}=1\times10^{16}$ 1/ m².s, (c) $g_{ae}=5\times10^{16}$ 1/ m².s, and (d) $g_{ae}=9\times10^{16}$ 1/ m².

3.1. Anion flux only

I-Anion Flux to ETL side

Here, we investigate anion flux to the ETL side at the scan rate of S= 1V/s. The anion flux rates were changed from 5×10^{15} 1/ m^2. s to 9×10^{16} 1/ m^2. s. Figure 3 shows the J-V characteristics for different anion flux rates, so it can be understood that by increasing the anion flux rate, the J_{sc} was decreased, and Voc was increased. The gradient of electric potential at ETL and contact sides for g_{ae}= 9×10^{16} 1/ m^2. s is stronger than the case of g_{ae}=5×10^{15} 1/ m^2. s, which causes the V_{oc} increment (Fig. 4(a)). The high recombination rate was seen for the case of g_{ae}= 9×10^{16} 1/ m^2. s, which leads to the lower J_{sc}, especially for the BS direction (Fig. 4(b)). Anions are accumulated at ETL near the contact (Fig. 4(c)), creating a barrier for charge carriers and increasing the recombination rate in the PSK layer. The cations distributions remain constant (Fig. 4(d)) during anions migration.

II-Anion Flux to HTL side

The effect of anion flux to the HTL side toward contacts was screened on J-V characteristics (Fig. 5). The values of g_{ah} were modified from 5×10^{15} 1/ m^2. s to 9×10^{16} 1/ (m^2. s). by increasing the g_{ah}, Voc increased due to a stronger gradient of electric potential (also electric field) at PSK/HTL sides (Fig. 6(a)). The recombination rate was increased for the case of g_{ah}= 9×10^{16} 1/ (m^2. s) from the middle of PSK to ETL side (Fig. 6(b)) due to anions accumulation in HTL and HTL contact side (Fig. 6(c)). The accumulation of anions at the HTL side creates stronger barriers to prevent carrier transport from perovskite to the HTL side and causes lower J_{sc} in perovskite solar cells. Cation distributions were unchanged (Fig. 6(d)).

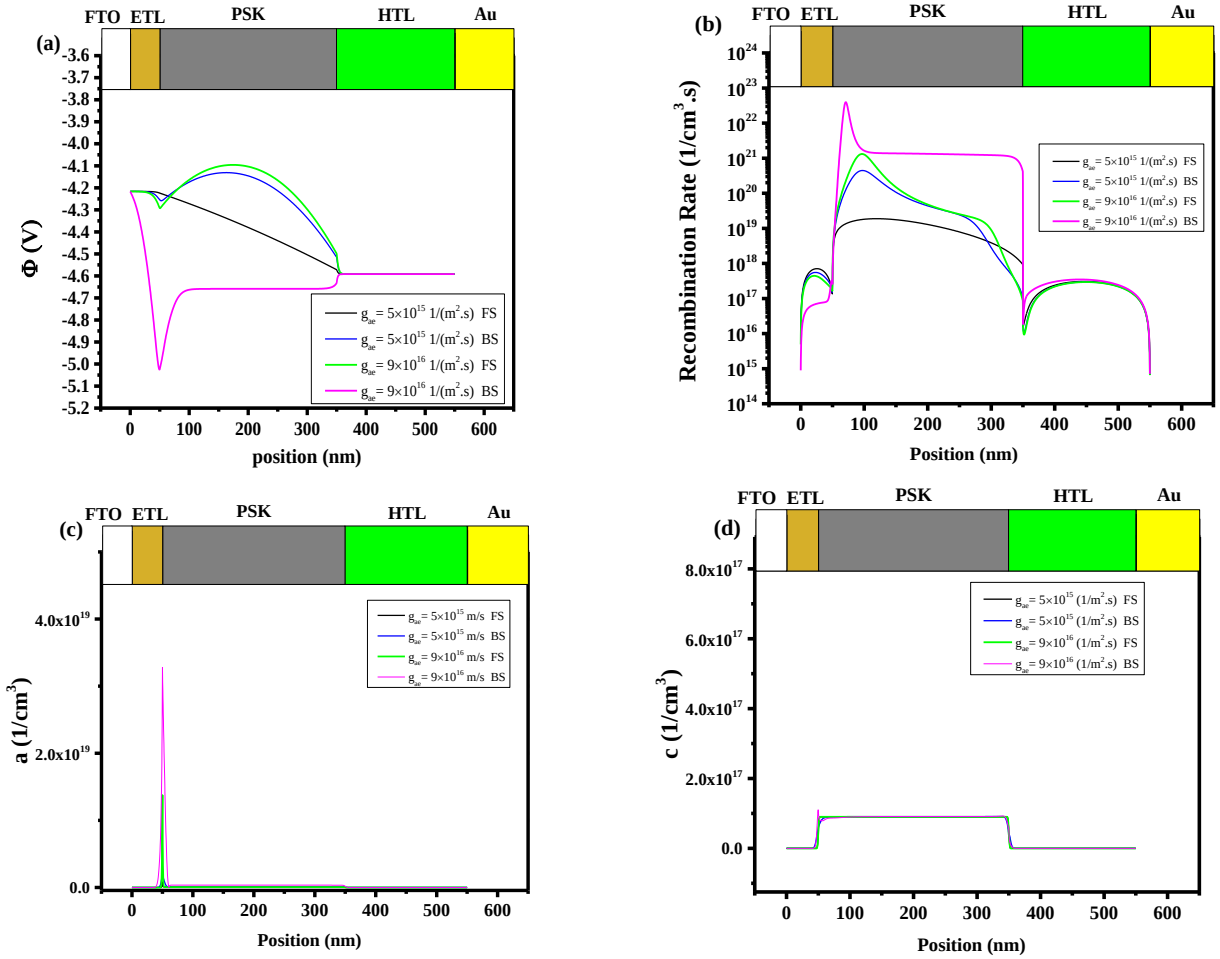

Fig. 4. Effect of different anion flux rates to ETL on (a) electric potential (b) recombination rate, (c) anion distribution, and (d) cation distribution for g_{ae}=5×10^{15} 1/(m^2.s) and g_{ae}=9×10^{16} 1/(m^2.s). Data were taken at 0.2 V (t= 0.192s (FS) and t= 2.208s (BS)).

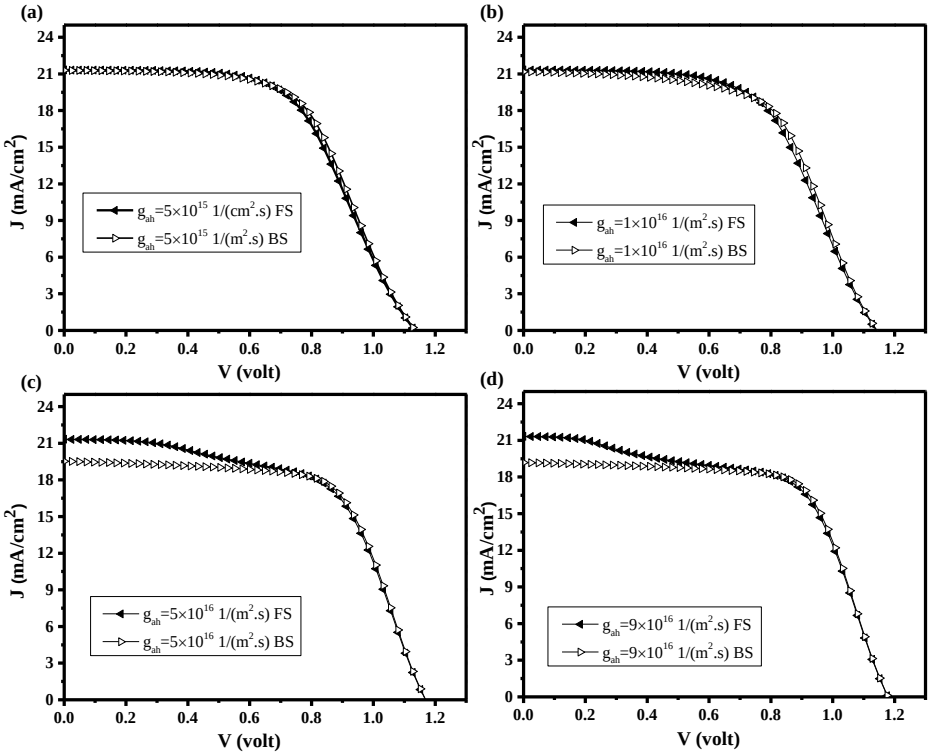

Fig. 5. Effect of different anion flux rates to HTL on J-V characteristics for (a) $g_{ah}=5\times10^{15}$ 1/ m².s, (b) $g_{ah}=1\times10^{16}$ 1/ m².s, (c) $g_{ah}=5\times10^{16}$ 1/ m².s, and (d) $g_{ah}=9\times10^{16}$ 1/ m².s

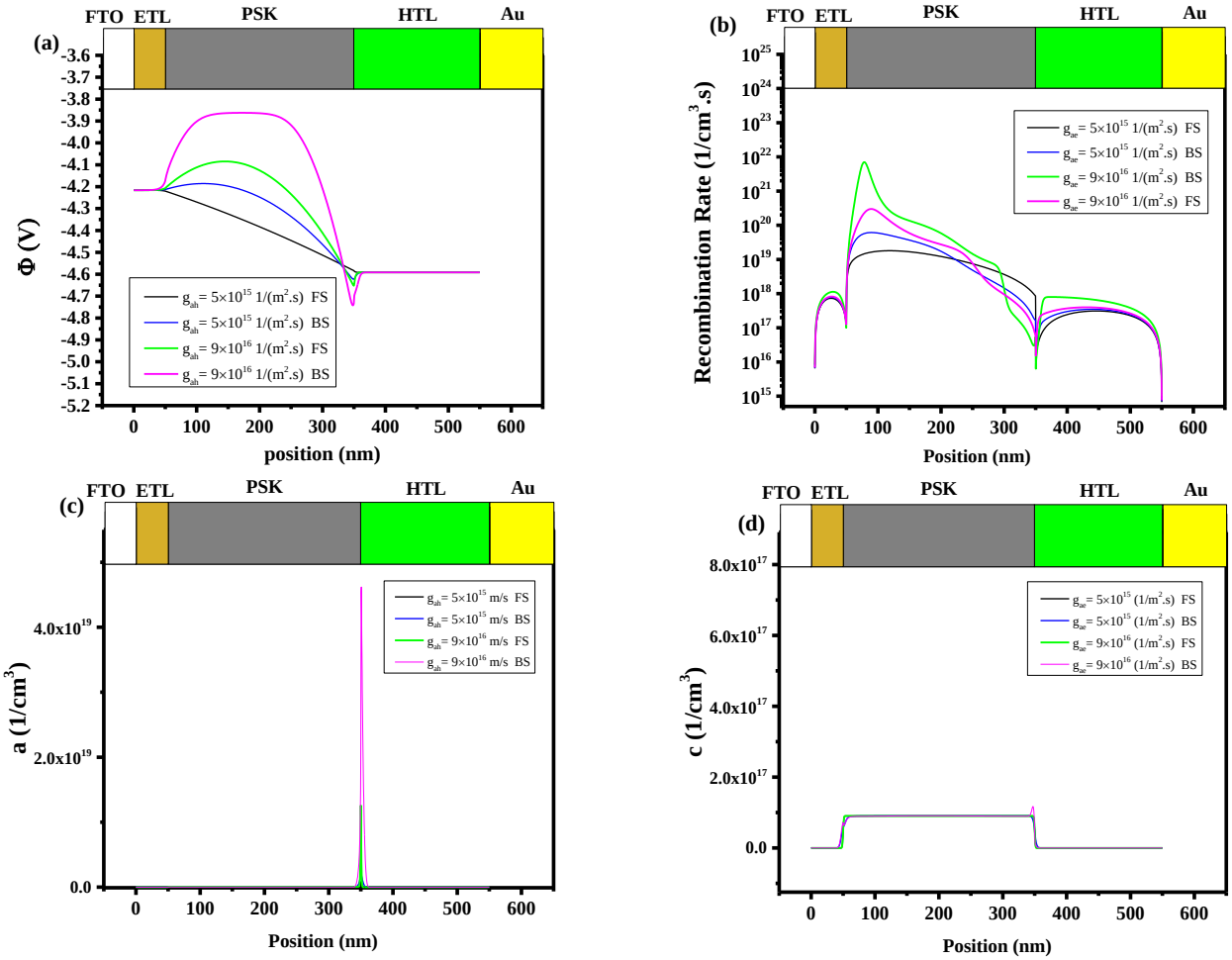

Fig. 6. Effect of different anion flux rates to HTL on (a) electric potential (b) recombination rate, (c) anion distribution, and (d) cation distribution for $g_{ah}=5\times10^{15}$ 1/(m².s) and $g_{ah}=9\times10^{16}$ 1/(m².s). Data were taken at 0.2 V (t= 0.192s (FS) and t= 2.208s (BS)).

3.2. Cation flux only

I-Cation Flux to ETL side

Here, the effect of cation flux to the ETL side on J-V characteristics (Fig. 7) was studied. By changing g_{ce} from 5×10^{15} 1/ m^2. s to 9×10^{16} 1/(m^2.s), the V_{oc}, FF, and efficiency were increased. The stronger gradient of electric potential in the middle of perovskite (Fig. 8(a)) caused the higher V_{oc} for the higher values of g_{ce}. The recombination rate (Fig. 8(b)) at the opposite side of cation accumulation (Fig. 8(d)) was increased, and it caused the J_{sc} decrement (a little change). Here, a reverse relation between cation distribution and recombination rate can be seen. Anion distribution remains constant at the PSK layer (Fig. 8(c)).

II-Cation Flux to HTL side

In this section, the effect of the cation migration to the HTL side on the J-V characteristics is studied. (Fig. 9). The values of V_{oc} increased with the increase of the g_{ch} as the gradian of electric potential at PSK/ETL and PSK/HTL was increased (Fig. 10(a)). While g_{ch} increased to the value of 9×10^{16} 1/ (m^2. s), J_{sc} decreased significantly, originating from the increment of recombination rate in the whole of the PSK layer, especially the PSK/HTL interface (Fig. 10 (b)). The anion distribution in the PSK layer was constant (Fig. 10(c)). The accumulation of cations at the HTL/PSK side causes a higher recombination rate in this region (Fig. 10(d)).

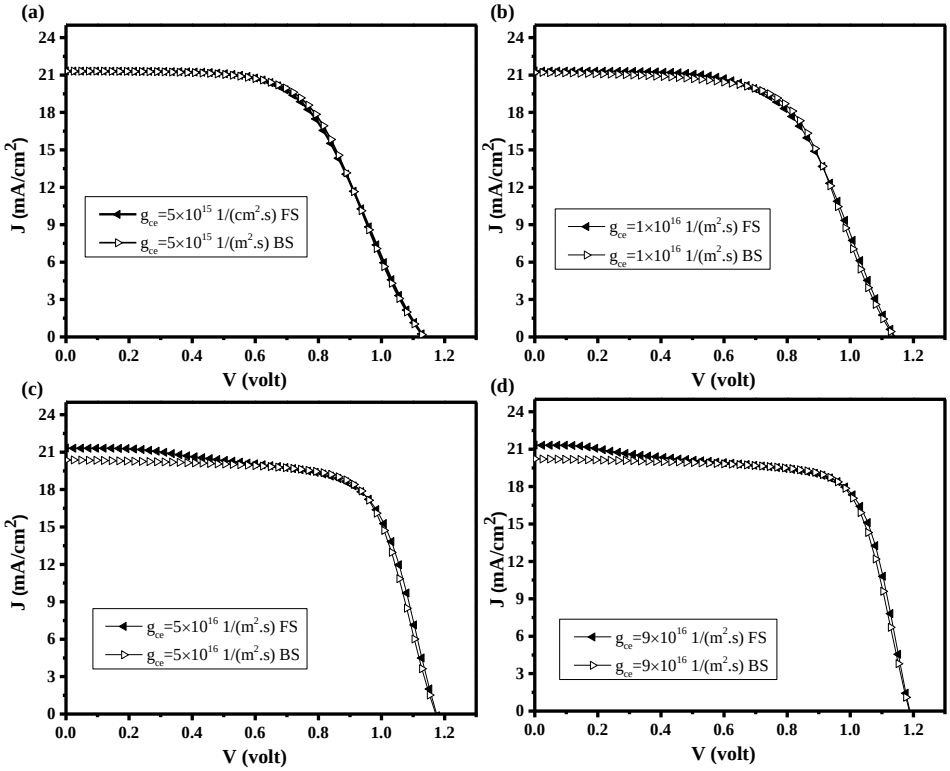

Fig. 7. Effect of different cation flux rates to ETL on J-V characteristics for (a) $g_{ce}=5\times10^{15}$ 1/ m^2.s, (b) $g_{ce}=1\times10^{16}$ 1/ m^2.s, (c) $g_{ce}=5\times10^{16}$ 1/ m^2.s, and (d) $g_{ce}=9\times10^{16}$ 1/ m^2.s.

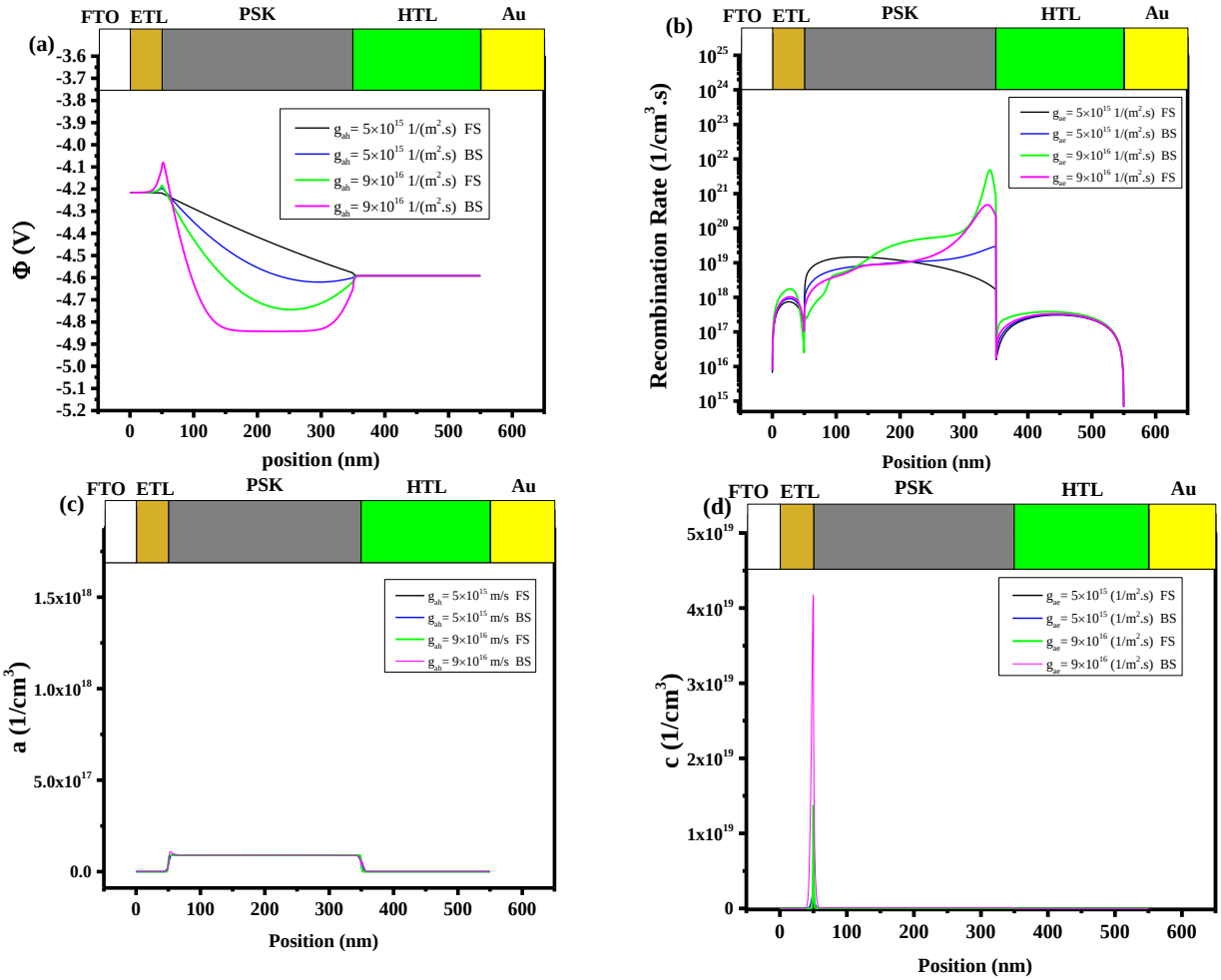

Fig. 8. Effect of different cation flux rates to ETL on (a) electric potential (b) recombination rate, (c) anion distribution, and (d) cation distribution for g_{ce}=5×10¹⁵ 1/(m².s) and g_{ce}=9×10¹⁶ 1/(m².s). Data were taken at 0.2 V (t= 0.192s (FS) and t= 2.208s (BS)).

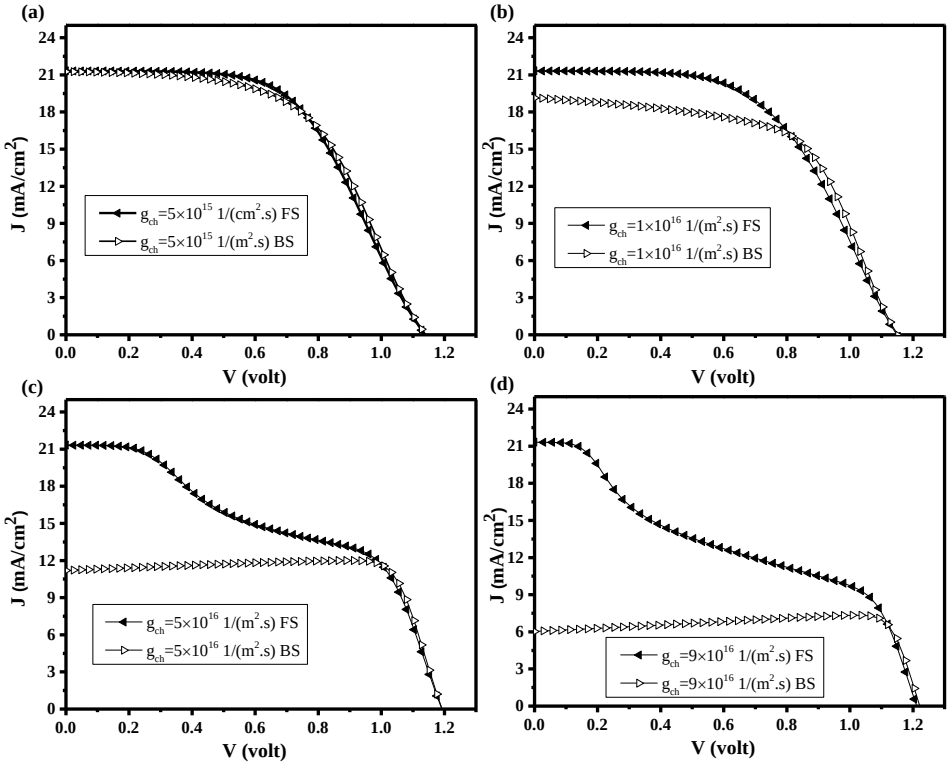

Fig. 9. Effect of different cation flux rates to HTL on J-V characteristics for (a) g_{ch}=5×10¹⁵ 1/ m².s, (b) g_{ch}=1×10¹⁶ 1/ m².s, (c) g_{ch}=5×10¹⁶ 1/ m².s, and (d) g_{ch}=9×10¹⁶ 1/ m².s

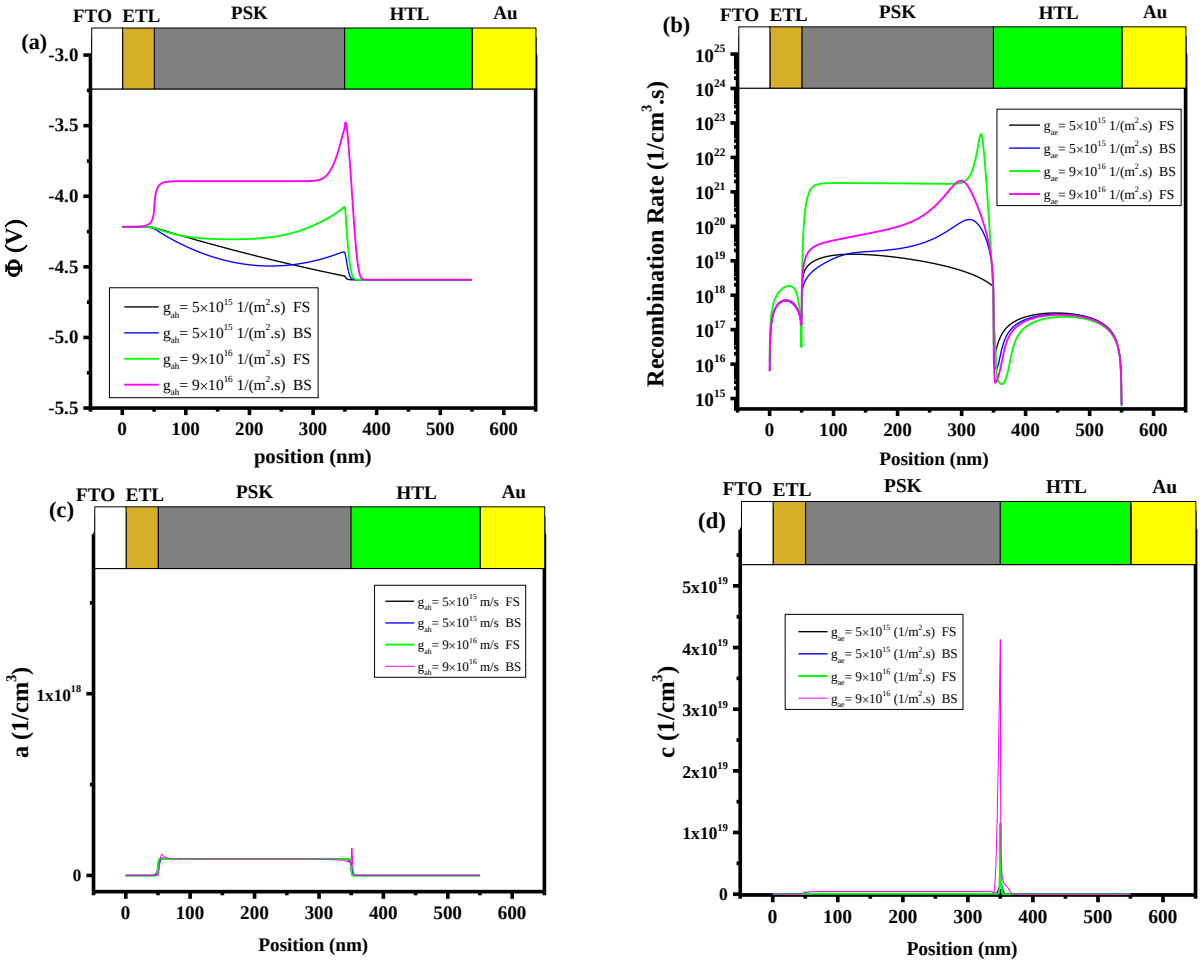

Fig. 10. Effect of different cation flux rate to HTL on (a) electric potential (b) recombination rate, (c) anion distribution, and (d) cation distribution for g_{ch}=5×10^{15} 1/(m^2.s) and g_{ch}=9×10^{16} 1/(m^2.s). Data were taken at 0.2 V (t= 0.192s (FS) and t= 2.208s (BS)).

4. Conclusion

In this paper, we have modelled the experimental J—V hysteresis of a perovskite solar cell by Free Fem Software. The hysteresis behavior by considering the conventional ionic migration transport equation was simulated. For the reference model, we used two types of ions (anions and cations). Then, we modified the common model of ionic migration by considering ionic flux that allowed ions to transport to other layers toward contacts. We considered two states for anions and cations migration, anion flux to ETL and HTL side near the contacts and cation flux to ETL and HTL side toward contacts. For the model of anion flux to the HTL side and cation flux to the ETL side, when the ionic flux rate increased, Voc, FF, and efficiency increased, but Jsc decreased slightly. The results show that for these models, the recombination centers are generated on the opposite side of the accumulated anions and cations. In the model of anion flux to the ETL side and cation flux to the HTL side, Jsc and efficiency decrease dramatically, and the recombination centers are created on the side of distributed anions and cations. Strong inverted hysteresis is observed in the case of anion flux to ETL and cation flux to HTL sides. For all ionic flux models, the Voc is increased due to the higher electric potential gradient at the ETL/PSK and HTL/PSK sides. This high gradient originated from the high density of accumulated anion and cation at ETL/PSK and HTL/PSK sides. We proposed some treatments of PSK/ETL and PSK/HTL interfaces, such as chemical interfacial passivation, annealing conditions, precursor aging, precursor temperature, additives in perovskite precursor solutions, and compositional engineering, to prevent anion and cation flux to ETL, and HTL, respectively and suppress hysteresis and degradation of the perovskite layer.

References

[1] J. Werner, C.C. Boyd, M.D. McGehee. "Perovskite-Based Multijunction Solar Cells." Perovskite Photovoltaics and Optoelectronics: From Fundamentals to Advanced Applications (2022) 433–453.

[2] N. Nikfar, N. Memarian. "Theoretical study on the effect of electron transport layer parameters on the functionality of double-cation perovskite solar cells." Optik 258 (2022) 168932.

[3] J. Zeng, Y. Qi, Y. Liu, D. Chen, Z. Ye, Y. Jin. "ZnO-Based Electron-Transporting Layers for Perovskite Light-Emitting Diodes: Controlling the Interfacial Reactions." The Journal of Physical Chemistry Letters 13 (2022) 694–703.

[4] Y.T. Li, L. Han, H. Liu, K. Sun, D. Luo, X.L. Guo, D.L. Yu, T.L. Ren. "Review on Organic–Inorganic Two-Dimensional

Perovskite-Based Optoelectronic Devices." ACS Applied Electronic Materials 4 (2022) 547-567.
[5] A. Kojima, K. Teshima, Y. Shirai, T. Miyasaka. "Organometal Halide Perovskites as Visible-Light Sensitizers for Photovoltaic Cells." Journal of the american chemical society 131 (2009) 6050–6051.
[6] https://www.nrel.gov/pv/cell-efficiency.html, (2022).
[7] T. Bu, J. Li, F. Zheng, W. Chen, X. Wen, Z. Ku, Y. Peng, J. Zhong, Y.-B. Cheng, F. Huang. "Universal passivation strategy to slot-die printed SnO2 for hysteresis-free efficient flexible perovskite solar module." Nature communications 9 (2018) 1–10.
[8] J. Wei, Q. Wang, J. Huo, F. Gao, Z. Gan, Q. Zhao, H. Li. "Mechanisms and suppression of photoinduced degradation in perovskite solar cells." Advanced Energy Materials 11 (2021) 2002326.
[9] O. Almora, P. Lopez-Varo, K.T. Cho, S. Aghazada, W. Meng, Y. Hou, C. Echeverría-Arrondo, I. Zimmermann, G.J. Matt, J.A. Jiménez-Tejada. "Ionic dipolar switching hinders charge collection in perovskite solar cells with normal and inverted hysteresis." Solar Energy Materials and Solar Cells 195 (2019) 291–298.
[10] A. Singh, W. Kaiser, A. Gagliardi. "Role of cation-mediated recombination in perovskite solar cells." Solar Energy Materials and Solar Cells 221 (2021) 110912.
[11] G.A. Nemnes, C. Besleaga, V. Stancu, D.E. Dogaru, L.N. Leonat, L. Pintilie, K. Torfason, M. Ilkov, A. Manolescu, I. Pintilie. "Normal and inverted hysteresis in perovskite solar cells." The Journal of Physical Chemistry C. 121 (2017) 11207–11214.
[12] M. Minbashi, E. Yazdani. "Comprehensive study of anomalous hysteresis behavior in perovskite-based solar cells." Scientific Reports 12 (2022) 1–14.
[13] H. Li, R. Yang, C. Wang, Y. Wang, H. Chen, H. Zheng, D. Liu, T. Zhang, F. Wang, P. Gu. "Corrosive Behavior of Silver Electrode in Inverted Perovskite Solar Cells Based on Cu: NiO x." IEEE Journal of Photovoltaics 9 (2019) 1081–1085.
[14] X. Li, S. Fu, W. Zhang, S. Ke, W. Song, J. Fang. "Chemical anti-corrosion strategy for stable inverted perovskite solar cells." Science advances 6 (2020) eabd1580.
[15] https://freefem.org/, (n.d.).
[16] M. Burgelman, J. Verschraegen, S. Degrave, P. Nollet. "Modeling thin-film PV devices." Progress in Photovoltaics: Research and Applications 12 (2004) 143–153.
[17] M. Burgelman, J. Verschraegen, B. Minnaert, J. Marlein. "Numerical simulation of thin film solar cells: practical exercises with SCAPS." Proceedings of NUMOS. University of Gent. (2007) 357–366.
[18] Y. Kawano, J. Chantana, T. Minemoto. "Impact of growth temperature on the properties of SnS film prepared by thermal evaporation and its photovoltaic performance." Current Applied Physics 15 (2015) 897–901.
[19] A. Ghobadi, M. Yousefi, M. Minbashi, A.H.A. Kordbacheh, A.R.H. Abdolvahab, N.E. Gorji. "Simulating the effect of adding BSF layers on Cu2BaSnSSe3 thin film solar cells." Optical Materials 107 (2020) 109927.
[20] S.J. Fonash. "Chapter Two - Material Properties and Device Physics Basic to Photovoltaics, in: S.J.B.T.-S.C.D.P. (Second E. Fonash (Ed.)." Academic Press, Boston (2010) 9–65.
[21] M. Burgelman. "Mott-Schottky analysis from C-V simulations, and Admittance Analysis from C-f simulations in SCAPS." in: Dept. of Electronics and Information Technology (ELIS) University of Gent 'Belgium' (2017) 2–4.
[22] Y. Park, S. Lee, J. Yi, B.-D. Choi, D. Kim, J. Lee. "Sputtered CdTe thin film solar cells with Cu2Te/Au back contact." Thin Solid Films 546 (2013) 337–341.
[23] S.M. Sze, K.K. Ng. "Physics of semiconductor devices, John wiley & sons." (2006).
[24] M. Minbashi, A. Ghobadi, M.H. Ehsani, H. Rezagholipour Dizaji, N. Memarian. "Simulation of high efficiency SnS-based solar cells with SCAPS." Solar Energy 176 (2018) 520–525.
[25] M. Minbashi, M.K. Omrani, N. Memarian, D.H. Kim. "Comparison of theoretical and experimental results for band-gap-graded CZTSSe solar cell." Current Applied Physics 17 (2017) 1238–1243.
[26] M. Minbashi, E. Yazdani. "Comprehensive study of anomalous hysteresis behavior in perovskite-based solar cells." Scientific Reports 12 (2022) 1–14.
[27] C. Multiphysics. "Comsol Multiphysics." Reference Manual: Version 5.6 (2014).
[28] F. Wu, R. Pathak, K. Chen, G. Wang, B. Bahrami, W.H. Zhang, Q. Qiao. "Inverted current–voltage hysteresis in perovskite solar cells." ACS Energy Letters 3 (2018) 2457–2460.
[29] W. Li, M.U. Rothmann, Y. Zhu, W. Chen, C. Yang, Y. Yuan, Y.Y. Choo, X. Wen, Y.-B. Cheng, U. Bach. "The critical role of composition-dependent intragrain planar defects in the performance of MA1–xFAxPbI3 perovskite solar cells." Nature Energy 6 (2021) 624–632.
[30] F. Wu, R. Pathak, K. Chen, G. Wang, B. Bahrami, W.H. Zhang, Q. Qiao. "Inverted current–voltage hysteresis in perovskite solar cells." ACS Energy Letters 3 (2018) 2457–2460.